Heat Transfer to a Hemisphere-Cylinder at Low Reynolds Numbers

R. S. HICKMAN*
Heliodyne Corporation, Westwood, Calif.
AND
W. H. GIEDT†
University of California, Berkeley, Calif.

Measurements of the local heat flux to hemisphere-cylinder models in a supersonic rarefied air stream are presented. Two different steady-state methods were developed, and five individual models were used. Data were obtained throughout the Mach number range of 2 to 6, with Reynolds numbers (based on conditions behind the bow shock and model diameter) varying from 38 to 1730. The stagnation point data indicated a gradual increase from continuum boundary layer theory at the higher Reynolds numbers to about 10% above at the lower end of the range investigated. Pressure distribution measurements on cooled and uncooled models were found to agree well with modified Newtonian theory. Local recovery factor measurements showed a small rarefaction effect at the lowest Reynolds numbers.

Nomenclature

c = sound speed
C_p = pressure coefficient = $(p - p_s)/\frac{1}{2}\rho_s U_s^2$
c_p = specific heat
D = model diameter
F = heat flux potential = $\int_{t_i}^{t} k dt$
H = specific gas total enthalpy
h = convective heat transfer coefficient
k = thermal conductivity
M = Mach number = U/c
Nu = Nusselt number = hD/k
p = gas pressure
Pr = Prandtl number
q = heat flux per unit area
R = recovery factor = $(t_{aw} - t_\infty)/(t_0 - t_\infty)$, and perfect gas constant
Re = Reynolds number = $(UD\rho)/\mu$
r = local radius
s = curvilinear distance from stagnation point
t = local temperature in gas or in model
u = velocity parallel to surface
u_e = velocity outside boundary layer
U_s = velocity behind bow shock
$\tilde{u}_s'$ = nondimensional velocity gradient outside boundary layer
U_∞ = freestream gas velocity
v = velocity normal to surface
y = distance normal to body surface
β = du_e/ds
γ = ratio of specific heats
δ = wall thickness of nickel model
ϵ = density ratio across normal shock
θ = local angle measured from model stagnation point
μ = viscosity
ν = kinematic viscosity = μ/ρ
ρ = density

Subscripts

∞ = freestream condition
θ = at θ
BL = from boundary layer analysis
c = corrected
e = edge of boundary layer
g = glass
0 = stagnation point or freestream stagnation condition
s = condition behind shock

Received by IAS August 17, 1962; revision received December 17, 1962. This paper is based on work supported by the Aeronautical Research Laboratory of the Air Force Aeronautical Systems Division, Wright Field, Ohio.

* Research Engineer.

† Professor of Aeronautical Sciences.

Introduction

ALTHOUGH substantial progress has been made toward an understanding of hypersonic flow around a blunt body in the free molecular and continuum flow regimes, adequate experimental and theoretical interpretations of the transition region [$1 \gtrsim (M_\infty/R_\infty) \to 0.01$] are lacking. Contrary to initial opinion, it appears that a modified boundary layer approach may be possible.[1] It will, however, be necessary to account for second-order effects, ordinarily neglected in classical boundary layer theory. In particular, it has been suggested that the vorticity introduced as the flow passes through the curved bow shock wave will influence the skin friction and heat transfer. Other effects are slip and temperature jump, boundary layer displacement of the flow, and body curvature.

Considerable attention therefore is being given to this "transition zone." Of the analytical studies in which heat transfer has been considered, two distinguishable approaches have been investigated. The first, used by Probstein,[2] Hoshizaki,[3] Ho and Probstein,[4] and Cheng,[5] was based on treating the flow between the body and the bow shock as a single region. Probstein and Hoshizaki assume the flow between the shock and the body to be incompressible. Hoshizaki also included slip and temperature jump in his boundary conditions but found their effects to be much less important than the density ratio across the shock wave. Their results include the stagnation point heat transfer and skin friction variation with Reynolds number. To assess the importance of the second-order effects, comparisons with continuum boundary layer results also are made. Probstein, Hoshizaki, and Ho and Probstein obtain similar results showing a gradual increase with decreasing Reynolds number (for values of $Re_s = U_s D\rho_s/\mu_s \lesssim 1000$) over continuum boundary layer theory. The magnitude of the increase is dependent on the freestream velocity or density ratio across the shock. Cheng, however, predicts an increase over boundary layer theory starting at values of $Re_s \cong 20{,}000$. In the range of $100 < Re_s < 1000$, his results show approximately twice the increase as, for example, do those of Ho and Probstein.

The second approach was taken by Ferri, Zakkay, and Ting[6] and by Van Dyke.[7] Their procedure was to define two regions between the shock and the body. The flow in the region near the body is assumed to be viscous and that near the shock to be inviscid. Boundary conditions include specification of matching requirements at the interface. Both analyses predict an increase in heat transfer. Van Dyke's results are comparable to those of Ho and Probstein. The

increase predicted by Ferri et al., however, is from 200 to 300% higher, which is in general agreement with the results of Cheng. Stagnation point heat transfer data that agree with the latter theories also have been presented by Ferri et al.[6, 8]

In view of this apparent lack of agreement on the magnitude and region in which second-order effects are significant, it has been suggested[7] that, in particular, additional experimental results are needed. It was with this objective that the present investigation was undertaken. The low density wind tunnel at the University of California in Berkeley can provide steady flow conditions in the upper portion of the transition region. Two types of hemisphere-cylinder models were developed for local heat transfer measurements, and data were obtained in the Mach 2 to 6 and Reynolds number (based on conditions downstream of the shock and model diameter) 38 to 1720 ranges. Thin-walled glass models were used to determine recovery temperature distributions. Since the velocity gradient at the stagnation point is of importance in the classical boundary layer analysis, the pressure distributions on the hemisphere-cylinders were measured also. Simple pressure probes were used, and the results were found to agree with the modified Newtonian pressure coefficient distribution.

A brief review of previous theoretical and experimental work is presented in the following section to provide a basis for comparison of the results obtained. The experimental procedures and results then are described.

Prior Theoretical and Experimental Investigations

Slip Flow Regime Analyses

Fundamental interest and design needs have stimulated considerable analytical effort directed toward the investigation of second-order effects such as vorticity and temperature jump in the slip flow regime. This involves simultaneous solution of continuity, momentum, and energy equations, which for an axisymmetric body aligned with the flow can be written as

Continuity

$$(\partial/\partial s)(\rho u r) + (\partial/\partial y)(\rho v r) = 0 \tag{1}$$

Momentum

$$\rho\left(u\frac{\partial u}{\partial s} + v\frac{\partial u}{\partial y}\right) = -\frac{dp_e}{ds} + \frac{\partial}{\partial y}\left(\mu\frac{\partial u}{\partial y}\right) \tag{2}$$

Energy

$$\rho\left(u\frac{\partial H}{\partial s} + v\frac{\partial H}{\partial y}\right) = \frac{\partial}{\partial y}\left(\frac{\mu}{Pr}\frac{\partial H}{\partial y}\right) + \mu\left[\left(1 - \frac{1}{Pr}\right)\frac{\partial}{\partial y}\left(\frac{u^2}{2}\right)\right] \tag{3}$$

where u and v are the velocities in the s and y directions parallel and normal to the surface, H is the local total enthalpy, and Pr is the Prandtl number. To the foregoing system must be added an equation of state, an equation describing the viscosity variation with temperature, and appropriate boundary conditions.

Since attention will be focused on deviations of solutions from conventional boundary layer conditions, reference is made first to established boundary layer results. Flow in the stagnation region behind the shock wave is subsonic and as a first approximation may be assumed to be incompressible. In this case, the analysis of Frössling[9] and the more limited stagnation region solution of Sibulkin[10] are applicable. Constant average thermal properties are assumed. Thermal property variation with temperature, the effects of diffusion and recombination, and compressibility were included in the analyses of Fay and Riddell.[11] A method for predicting the heat transfer distribution for hypersonic flow and a highly cooled surface was given by Lees.[12] For comparable conditions, all these analyses are in satisfactory agreement at the stagnation point. (Lees' result is about 6% lower than the others.)

Two different approaches have been followed in solving Eqs. (1–3) in the slip flow regime. The first, used by Hoshizaki,[3] Ho and Probstein,[4] and Cheng,[5] treats the flow between the body surface and the shock wave as a single region in which viscosity plays an important role.

Hoshizaki assumed incompressible flow but included the following slip and temperature jump boundary conditions at the wall:

$$u_{\text{wall}} = \lambda_w (\partial u/\partial y)_w$$

$$t_f = t_w + \left(\frac{2-\alpha}{\alpha}\frac{2\gamma}{\gamma+1}\frac{\lambda_w}{Pr}\right)_w \left(\frac{\partial t_f}{\partial y}\right)_w \tag{4}$$

where

u_w = gas velocity at wall
λ_w = mean free path at wall
t_f = gas temperature at wall
α = thermal accommodation coefficient

The inviscid strong shock relations given by

$$\begin{aligned} u_s &= U_\infty \sin\theta \\ v_s &= -\epsilon U_\infty \cos\theta \\ t &= t_s \end{aligned} \tag{5}$$

were applied at the outer boundary. The equations were solved numerically. Results showed the effect of shock-generated vorticity on heat transfer to approach 50% or more for density ratios across the shock less than 0.10. At higher ratios (for $M_\infty < 8$), the effect was of the order of 5% or less. The influence of wall slip was comparatively unimportant.

Ho and Probstein considered the flow to be compressible but assumed no slip at the body surface. The reduction of the Navier-Stokes equations to ordinary differential equations was carried out by assuming locally spherically symmetric solutions for the flow quantities of the form

$$\begin{aligned} \rho &= \rho_0(r) \\ q_\theta &= u(r)\sin\theta \\ q_r &= -v(r)\cos\theta \\ \mu &= \mu_9(r)\cos\theta \\ p &= p_0(r)\cos^2\theta + p_2(r)\sin^2\theta \\ H &= H_0(r)\cos^2\theta \end{aligned} \tag{6}$$

The strong shock relations were taken for the outer boundary conditions.

Cheng's approach is similar to conventional boundary layer analysis. He also assumes zero slip at the wall but adds tangential stress and heat conduction terms to the Hugoniot strong shock outer boundary conditions. His stagnation point heat transfer variation differs from those of Hoshizaki and Ho and Probstein in several respects. It indicates a vorticity effect at Reynolds numbers greater than 10,000 as compared to 1000. Also, the maximum magnitude of the effect is two to three times greater. Most interesting, however, is the fact that the curve increases with decreasing Reynolds number to a maximum and then decreases toward the curve for free molecule flow. All other theoretical results show a monotonically increasing trend with decreasing Reynolds number.

The second analytical approach has been to divide the flow between the surface and the shock wave into two distinct regions. The inner region is treated as a boundary layer, and the flow in the outer is assumed to be inviscid. This then requires specification of matching conditions at the interface.

The analysis of Ferri, Zakkay, and Ting[6] is based on matching of the tangential velocity and its gradient, the enthalpy and enthalpy gradient, and the mass flow at the edge of the

boundary layer. A solution for the entire region between the shock wave and body first is obtained assuming compressible inviscid flow. Next, the boundary layer transformations and simplifications employed by Lees[12] are introduced. A location where u and $\partial u/\partial y$ are the same for the two solutions then is determined subject to the matching of the mass flow in the boundary layer and the equivalent inviscid flow in the same region. Matching of the enthalpy and enthalpy gradient at the same value of y is not possible. This, however, is accomplished at a slightly greater distance from the wall. Zero slip at the body and the strong shock relations at the outer edge of the inviscid layer are the inner and outer boundary conditions. The magnitude of the vorticity effect predicted by Ferri et al. increases with Mach number or decreasing shock wave density ratio. At $M_\infty = 8$ the results are in good agreement with the increasing region of Cheng's result.

An investigation based on viscous and inviscid flow regions also has been carried out by Van Dyke.[7] The following second-order effects were considered: longitudinal curvature, transverse curvature, slip, temperature jump, entropy gradient, stagnation enthalpy gradient, and displacement. He uses inner and outer series expansions for the flow properties in terms of the variables y, s, and $\sigma \cong M_\infty/(R_\infty)^{1/2}$. The outer expansions for the inviscid flow take the form

$$\begin{aligned} u(s,y;\sigma) &\sim U_1(s,y) + \sigma U_2(s,y) + \dots \\ v(s,y;\sigma) &\sim V_1(s,y) + \sigma V_2(s,y) + \dots \\ &\vdots \end{aligned} \tag{7}$$

where U_1 and V_1 and U_2 and V_2 are the first- and second-order solutions for the velocities far from the wall. The inner expansions for the viscous region have the form

$$\begin{aligned} u(s,y;\sigma) &\sim u_1(s,y/\sigma) + \sigma u_2(s,y/\sigma) + \dots \\ v(s,y;\sigma) &\sim v_1(s,y/\sigma) + \sigma v_2(s,y/\sigma) + \dots \\ &\vdots \end{aligned} \tag{8}$$

where u_1 and v_1 and u_2 and v_2 are the first- and second-order solutions for the velocities near the wall. The pressure, density, and temperature are represented similarly.

Matching of the inner and outer solutions is accomplished by requiring at the matching interface for the first-order terms that

$$u_1(s,y/\sigma) \sim (y/\sigma)U_1(s,0) + U_2(s,0) \tag{9}$$
$$\vdots$$

and for the second-order terms that

$$u_2(s,y/\sigma) \sim (y/\sigma)U_1(s,0) + U_2(s,0) \tag{10}$$
$$\vdots$$

Van Dyke's numerical results for the heat transfer show an increase over conventional boundary layer solutions of about twice that of Ho and Probstein but only one half to one third that of Cheng or Ferri et al.

Slip Flow Regime Data

Experimental stagnation point heat transfer measurements in the vorticity interaction regime have been reported by Ferri and co-workers[6, 8] for freestream Mach numbers of approximately 6 and 8. These measurements were made in a blow-down-type tunnel using a transient technique. Values of the ratio $q_{w\text{vort}}/q_{w\text{vort}=o}$ were obtained by mounting a large diameter model in the tunnel stream along with smaller diameter models. The Reynolds number for the large model is high enough so that the vorticity effect on the heat transfer to it could be considered negligible. Values of $q_{w\text{vort}=o}$ then were computed for lower Reynolds numbers by assuming q to be proportional to $Re^{1/2}$. Measured values of q at the lower Reynolds numbers then were divided by these computed values.

Low density stagnation point heat transfer experiments also have been conducted in shock tunnels. Results in the range of interest have been reported by Neice and associates[13] and by Wilson and Wittliff.[14] The former were for density ratios varying from 0.1 to 0.07 and showed vorticity effects on the order of 50% at the lowest test density ratio (0.07) and Reynolds number (~200 based on conditions behind the shock and model diameter). The data showed considerable scatter, however, and are not very conclusive. Wilson and Wittliff compare their results to Cheng's theory. Although there is general agreement, the scatter of the data in the lower range of Reynolds numbers is such as to support equally well the results of Van Dyke or Ho and Probstein.

Experimental Equipment and Procedures

Tests were conducted in the low density wind tunnel at the University of California. This is a steady flow facility driven by steam ejectors, which are capable of pumping about 80 lb/hr of air at a pump inlet pressure of 80 μ. The air is drawn through a silica gel air dryer, through a flow rater, into a stagnation-settling chamber, through an axisymmetric de-Laval nozzle, into a plenum chamber, and finally into the pumping system. A complete description of the general tunnel instrumentation and flow characteristics is given in Refs. 15 and 16.

Two types of hemisphere-cylinder heat transfer models were developed. The first of these was thick-walled and made of a dielectric material with special instrumentation for measuring the inner and outer surface temperatures. The second was a thin-walled metal model in which the temperature variation through the wall was negligible. Both types were operated under steady-state conditions. A temperature difference between the models and the air stream was achieved by cooling the models with liquid nitrogen. Since the air stream total temperature was approximately 300°K, maximum differences of the order of 200°K thus were obtained.

Thick-Walled Dielectric Models

These models were based on the principle of determining the steady-state temperature distribution in the wall through which the heat flow is by conduction. Local convective heat flux to the outer surface then can be determined by evaluating the normal derivative of the temperature at this surface. The temperature distribution in the wall is obtained from the solution of the conduction equation using measured distributions along the inner and outer surfaces for the boundary conditions. This technique was applied successfully to a cylinder[17] by using resistance elements to measure surface temperatures. To adapt it to an axially symmetric body, however, use of thermocouple elements was considered preferable.

Models were made by first attaching pyrex tubing $\frac{1}{2}$-in.-o.d. to similarly sized Kovar tubing by a graded glass seal. Then tubing of the desired diameter was attached to the $\frac{1}{2}$-in. pyrex tube. The final step was to close this tube to form a hemispherical end. The wall thickness variation could be measured with a machinists microscope when the model was immersed in an oil that had the same index of refraction as the pyrex.

Local model outer surface temperatures were measured with silver-constantan thermocouples bonded to the surface (see Fig. 1). These thermocouples were prepared by first painting the model with a strippable lacquer. Then 0.010-in. strips were removed between the base and the desired location of the thermocouple junction. These strips were covered with silver paint, after which the remaining lacquer was removed. The paint then was fused to the pyrex by firing the model in an oven at 600°C. To complete each circuit, a 0.015 × 0.001-in. constantan ribbon was attached with a thin layer of silver paint at the end of each silver strip. Each constantan strip

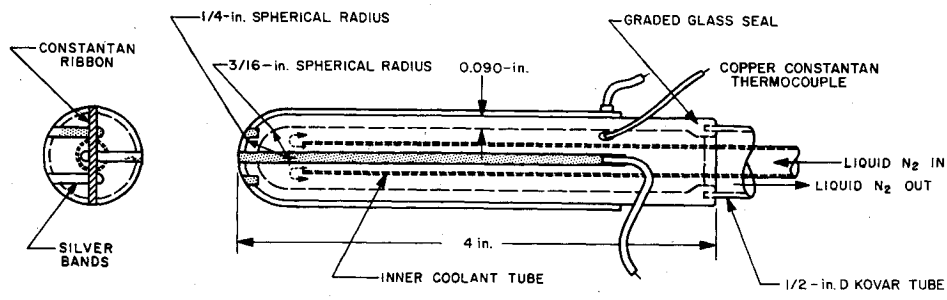

Fig. 1 Sketch of glass heat transfer model, 0.5-in.-diam

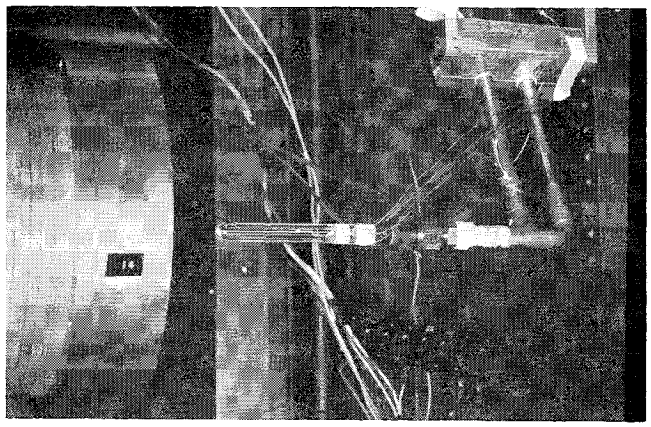

Fig. 2 Glass heat transfer model, 0.5-in.-diam, installed in the low density wind tunnel

was held against the model and bound around the base. It was found desirable to reference all temperatures to the base value that was measured with a copper-constantan junction. Copper leads were attached to the silver and constantan strips at the reference point on the base. These ultimately were brought out through the tunnel wall to a precision potentiometer.

Instrumentation of the inner surface was extremely difficult. It therefore was decided to make it essentially isothermal by coating with silver and forcing liquid nitrogen directly against it by means of an inner coolant tube (Fig. 1). Measurements at the inner stagnation point showed the surface to be about 0.5°K above the temperature of the impinging coolant. Figure 2 shows the 0.5-in. model as it was mounted for testing in the wind tunnel.

Several methods were tried for evaluating the local heat fluxes. The one finally used involved accounting for the temperature variation of the thermal conductivity by introduction of the conductivity potential $F = \int_{t_i}^{t} k dt$, local expansions for F in terms of the radius r, and the angle θ measured from the stagnation point. The procedure is described in detail in Ref. 18. Information about model thermocouple calibration also is given.

Thin-Walled Fin Models

A series of thin metal wall models was developed also to check the results obtained from the glass models. These operated like spherical fins and were made by electroforming nickel shells on aluminum forms. Wall thicknesses were on the order of 0.003 in. The nickel shells were soldered onto copper strings that were cooled with liquid nitrogen. Since under tunnel test conditions the inner surfaces of a shell should be considered insulated, aerodynamic heat input to the outer surface was conducted through the wall to the cooled sting. A heat balance on a ring-shaped element $\theta°$ from the stagnation point then yields for the local convective heat flux q_θ

$$q_\theta = \frac{k\delta}{r^2 \sin\theta}\left[\frac{d}{d\theta}\left(\sin\theta \frac{dt}{d\theta}\right)\right] \tag{11}$$

where k is the thermal conductivity of the model material, δ its wall thickness, and r the average radius. Assuming that k and δ are known, q_θ can be evaluated if t is measured as a function of θ.

The temperature distribution was determined by installing 0.003-in.-diam copper wires in the nickel shells at 10° intervals from the stagnation points. Thermocouple junctions thus were formed with the nickel wall at these locations. As before, the model base was used as a reference. Sketches of typical models are shown in Fig. 3. The 1-in. model as mounted in the wind tunnel is shown in Fig. 4.

Calibration of the copper-nickel thermocouple junctions and measurement of the wall thermal conductivity were found necessary. Details of the procedures used and methods for evaluating the temperature derivatives are given in Ref. 18.

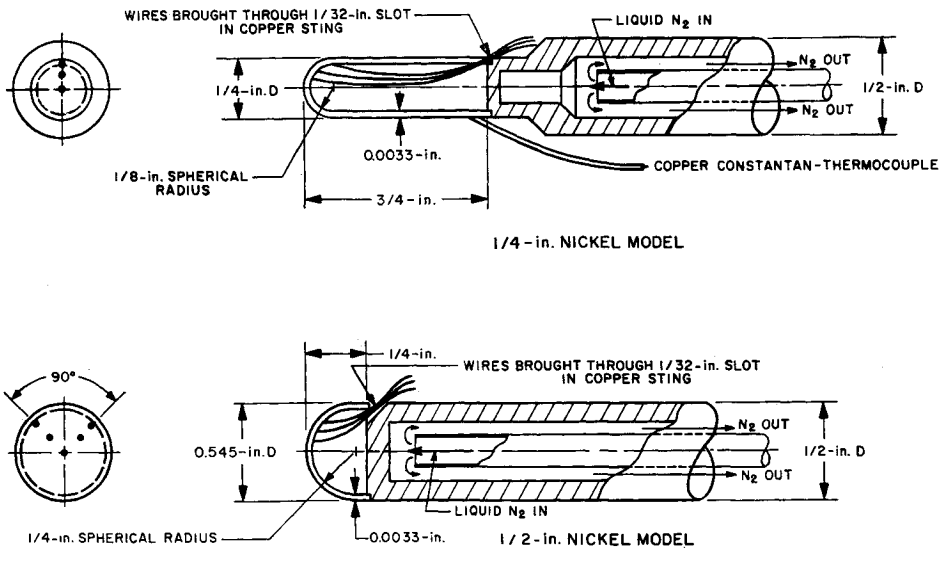

Fig. 3 Nickel heat transfer Models

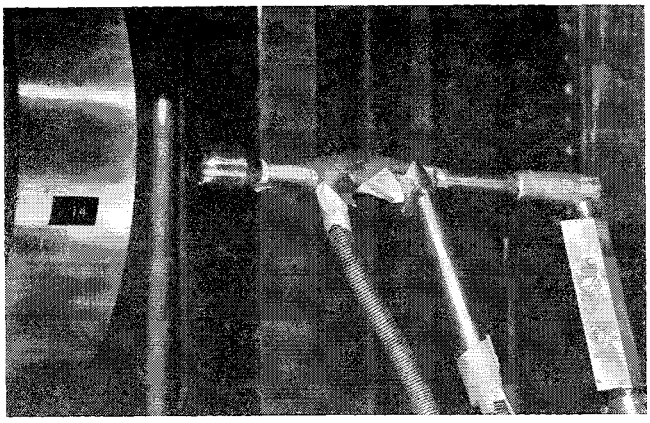

Fig. 4 Nickel heat transfer model, 1.0-in. diam, installed in tunnel

Recovery Factor Model

Recovery temperature distributions were measured with a model similar to the pyrex heat transfer models except that the wall thickness was reduced to 0.005 in. (see Fig. 5). Even with this comparatively thin wall, some conduction in the θ direction occurred. This introduced an error of less than 1%, for which a correction was made.[18]

Pressure Distribution Measurements

Two sets of models were used. The first consisted of seven $\frac{1}{2}$-in.-diam and the second of seven 1-in.-diam models. Except for the stagnation point model, each model had four equally spaced $\frac{1}{64}$-in.-diam holes drilled at one angular location. In the $\frac{1}{2}$-in. set, the first model had a $\frac{1}{32}$-in.-diam hole at the stagnation point; the second had four equally spaced $\frac{1}{64}$-in. diam holes located at 15° increments from the stagnation point; the remaining models each had four such holes located at multiples of 15° from the stagnation point.

The copper cylinders of the $\frac{1}{2}$-in. models were soldered to stainless steel tubes, which in turn were mounted to a rotating-type manifold. They were cooled by liquid nitrogen. This was achieved by soldering a copper block through which the nitrogen flowed far back on the cylindrical base of each model. Flexible copper tubes, soldered to each block, were connected to inlet and outlet coolant pipes that passed through the tunnel wall.

The 1-in.-diam models were built primarily to determine accurately the local pressure gradient near the stagnation point. For this reason, more local pressure measurements were made near the stagnation point than with the $\frac{1}{2}$-in. models. The angular pressure tap positions were 0°, 5°, 10°, 20°, 30°, 45°, and 60°. Data were taken only at Mach 6 for three flow rates without cooling.

Experimental Results

Several different formulations of the Reynolds number have been used in presenting results for heat transfer to a blunt body in hypersonic flow. The one used in this paper, which is based on conditions just downstream of the normal part of the bow shock, has been found to provide the most satisfactory correlation of the experimental results. It is given by

$$Re_s = U_s\rho_s D/\mu_s \tag{12}$$

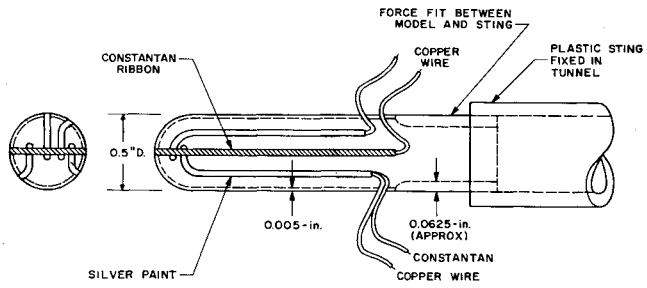

Fig. 5 Sketch of glass recovery factor model

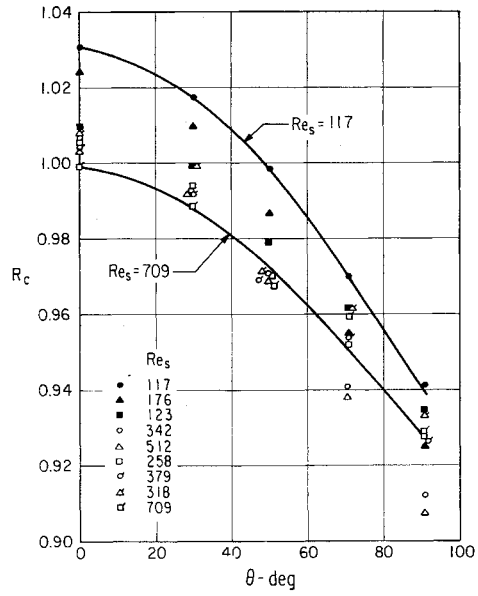

Fig. 6 Corrected recovery factor data vs θ

Recovery Factor Distributions

The local recovery factor was defined in terms of the temperature of an adiabatic surface in the flow by

$$R = (t_{aw} - t_\infty)/(t_0 - t_\infty) \tag{13}$$

where

t_{aw} = local adiabatic wall temperature
t_0 = stagnation temperature
t_∞ = freestream temperature

Values of the local recovery factors corrected for model wall conduction effects are plotted in Fig. 6. As can be seen, they increase with decreasing values of the Reynolds number. The rate of increase is rather small, however, as is shown in Fig. 7, where R_c has been plotted vs the Reynolds number behind the shock for θ = 0°, 45°, and 90°. The corrected stagnation point recovery factor is represented to within ±2% by the expression

$$R_c = 1 + 0.098(Re_s)^{1/2} \tag{14}$$

which implies the incipience of rarefaction effects.

Pressure Distributions

The local pressure coefficient C_p was defined as

$$C_p = (p - p_s)/\tfrac{1}{2}\rho_s U_s^2 \tag{15}$$

where p is the local pressure at model surface, and p_s, ρ_s, and U_s are for conditions downstream of the shock. The stagnation point coefficient was calculated for each flow setting from the Rankine-Hugoniot shock relations, and the ratio $C_p/C_{p_{max}}$ then was calculated for each angular position.

The measured pressure coefficient distributions are compared with the modified Newtonian pressure coefficient distribution in Fig. 8. Near the stagnation point, the observed distributions are in good agreement with the modified Newtonian curve. Beyond θ = 45°, however, deviations will be noted for M_∞ = 4 and 6. This is surprising, in that better overall agreement with the Newtonian expression would be expected at the higher Mach numbers.

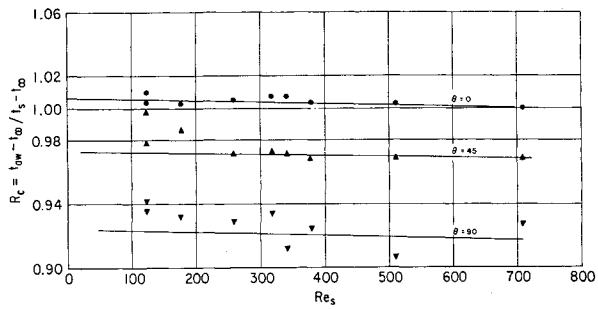

Fig. 7 Corrected recovery factor vs Re_s

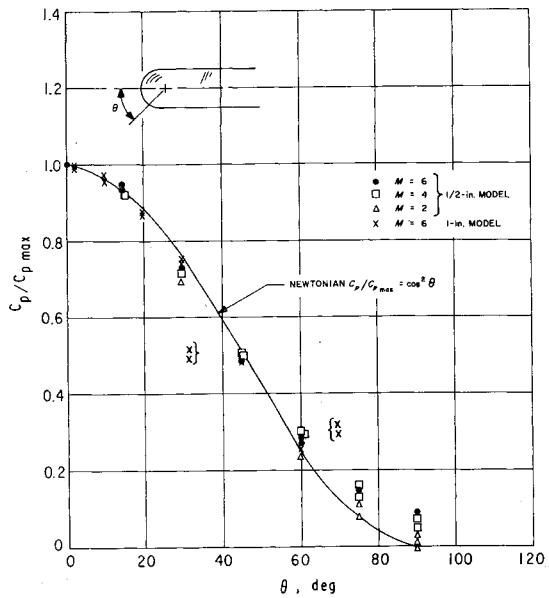

Fig. 8 Pressure coefficient ratio vs θ

There does not seem to be a strong Reynolds number effect on the pressure distribution. As Reynolds number was reduced, the local value of $C_p/C_{p_{max}}$ appeared to decrease slightly, although the trend hardly was more than the data scatter. Actually, this trend seems to be related more closely to the Mach number than to the Reynolds number; however, again definite conclusions cannot be made.

As might be expected, virtually no difference in pressure distribution was observed between tests for adiabatic or cold wall models. Tewfik and Giedt[17] report similar results for a cylinder.

Heat Transfer Results

The heat transfer coefficient at the stagnation point was calculated according to the equation

$$h_0 = q_0(t_0 - t_{w0}) \tag{16}$$

in which the recovery factor is assumed to be one. This approximation does not introduce serious error, since the greatest recovery factor expected (corresponding to the lowest Reynolds number) is approximately 1.014. Thus, at worst, a $1\frac{1}{2}\%$ error is introduced by assuming a recovery factor of one. Local heat fluxes, recovery temperatures, and wall temperatures were substituted in Eq. (16) to obtain local heat transfer coefficients.

The Nusselt number was defined as

$$Nu = hD/k_s \tag{17}$$

where k_s is the thermal conductivity of the gas directly behind the shock and is obtained from the data presented by Hilsenrath.[19]

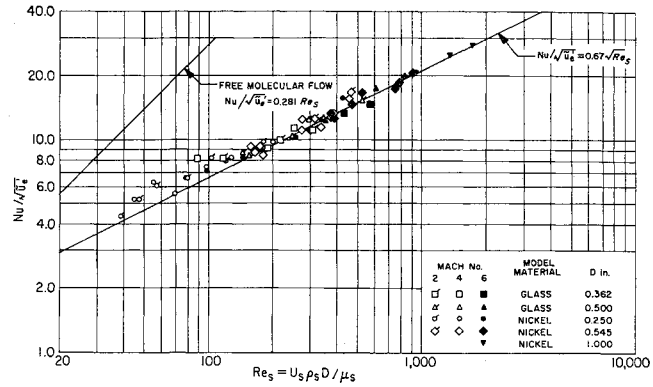

Fig. 9 $Nu/(\tilde{u}_e')^{1/2}$ Re_s for all models

To eliminate the Mach number effect, the stagnation point Nusselt number was divided by the square root of the nondimensional velocity gradient, $(\tilde{u}_e')^{1/2} = [d(u_e/U_s)/d(s/D)]^{1/2}$ Since the Newtonian pressure distribution $C_p/C_{p_{max}}$ was found to apply, $\tilde{u}_e'$ is related to M_∞ according to

$$\tilde{u}_e' = 2M_\infty(\gamma + 1)\left\{\left[\frac{M_\infty^2 - 1}{1 + [(\gamma - 1)/2]M_\infty^2}\right] \times \left[\frac{1}{2\gamma M_\infty^2 - (\gamma - 1)}\right]\right\}^{1/2} \tag{18}$$

For the present test conditions, $\gamma = 1.4$ is applicable.

The stagnation point heat transfer results are plotted in Fig. 9 vs the Reynolds number based on conditions im-

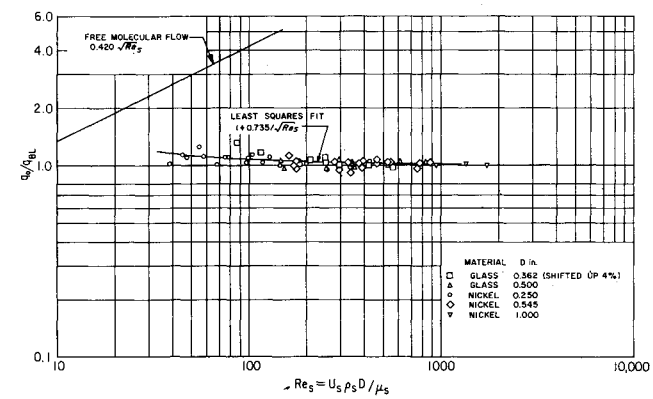

Fig. 10 Comparison of measured heat transfer rates with boundary layer values

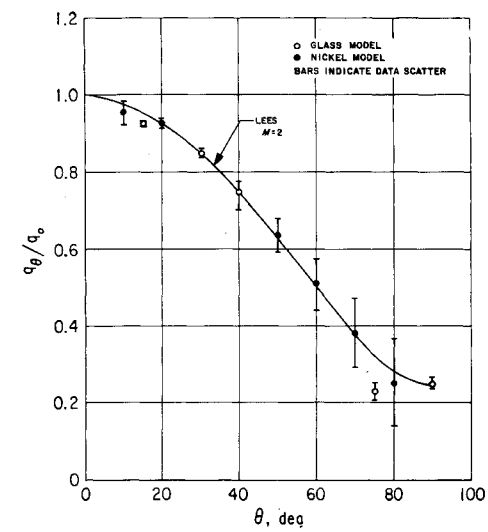

Fig. 11 Heat transfer distribution around hemisphere for $M_\infty = 2$

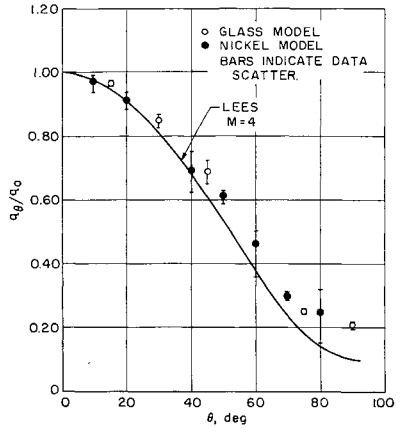

Fig. 12 Heat transfer distribution around hemisphere for $M_\infty = 4$

mediately behind the shock. The curve representing continuum boundary layer theory,[10, 11] $Nu/(\tilde{u}_e')^{1/2} = 0.67(Re_s)^{1/2}$, is included for comparison. Also included is a curve for free molecular flow heat transfer. As can be seen, agreement with theory occurs at Reynolds numbers greater than 500. Below this value, an increase over boundary layer theory is evident. It should be noted that the data presented were obtained from five separate models, three of which were nickel and two glass. Even if a consistent error of 5 to 10% existed in one set of models, it would be extremely unlikely for this error to exist in the other set. Thus one is led to believe that the data are accurate to within the data scatter. The uncertainty in the experimental results has been estimated[18] to be 7%, which is consistent with the observable scatter.

Figure 10 is a plot of the data of Fig. 9 compared to the boundary layer curve, with the 0.362-in.-diam glass model data shifted up by 4%.‡ A least squares data fit yields

$$\frac{q_0}{q_{BL}} = \frac{Nu/(\tilde{u}_e')^{1/2}}{Nu_{BL}/(\tilde{u}_e')^{1/2}} = 1 + \frac{0.735}{(Re_s)^{1/2}} \qquad (19)$$

which compares well with the equation given by Van Dyke:[7]

$$q_0/q_{BL} = 1 + [0.868/(Re_s)^{1/2}] \qquad (20)$$

The local heat transfer distributions normalized with respect to those of the stagnation point are given in Figs. 11–13 for nominal Mach numbers of 2, 4, and 6, respectively. The data shown cover the same range of Reynolds numbers as the stagnation points results but are not plotted as a function of the Reynolds number, since discernable variations are lacking. The vertical bars indicate the data scatter and show that the data uncertainty increases with distance from the stagnation point. This is to be expected, since the local heat flux at $\theta = 90°$ decreases to about 15% of the stagnation point heat flux. The data reduction was halted at $\theta = 80°$ for the nickel models, since the data scatter at this angle for these models became excessive. The local glass model data exhibit considerably less scatter than those of the nickel models and are felt to be more reliable.

The local heat flux predicted by Lees' method also is plotted in Figs. 11–13. The data agree well with the theory except for the Mach 6 results, which fall above the theoretical curve for $\theta > 45°$.

Discussion of Results and Conclusions

A summary of theoretical and experimental results is presented in Fig. 14. As may be noted, a least squares fit of the

‡ Data at the higher Reynolds numbers for this model were consistently below conventional boundary layer theory by about this amount. This was believed to be due to a systematic error, since other model results showed good agreement with this theroy.

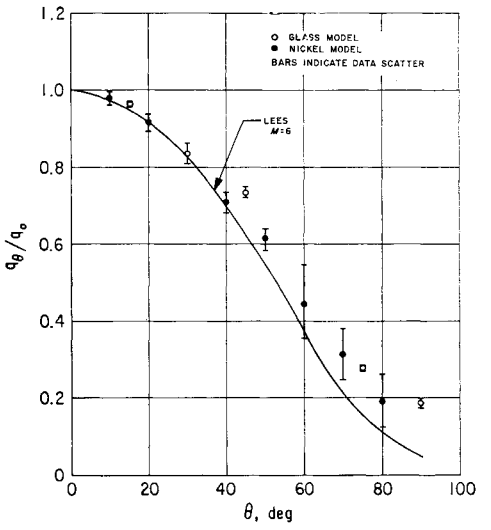

Fig. 13 Heat transfer distribution around hemisphere for $M_\infty = 6$

data of this report agrees well with Van Dyke's analysis. The data of Ferri et al. are significantly higher than the present data and deviate from conventional boundary layer theory at a Reynolds number greater than 10,000. This result is consistent with the theoretical prediction of Cheng but differs from other analyses, which show vorticity effects to become important at values of Reynolds numbers less than 2000.

It is clear from Fig. 14 that, if the experimental uncertainties in the present data are considered to enter randomly, the theory of Van Dyke is very nearly exactly represented by the data curve. His analysis indicates that the vorticity effect partially is compensated for by the temperature jump effect. If the latter effect is not included, the deviation from boundary layer theory shown in Fig. 14 would be shifted upward by about 40%. This is noteworthy since, without the temperature jump effect, the theoretical results of Hoshizaki, Ho and Probstein, and Van Dyke would deviate from one another more markedly than is indicated. If the additional effect of temperature jump were applied to the results of Ho and Probstein, their theoretical predictions would fall considerably below the present data.

In addition to the different boundary conditions employed in the several theories, some variation in the results may be attributable to how viscosity was assumed to vary with temperature. For example, Cheng, Ferri et al., and Van Dyke considered $\mu \sim t$, whereas Ho and Probstein assumed $\mu \sim t^{1/2}$.

Since it is difficult, if not impossible, to isolate the effects of such variations between the several theories, numerical comparisons must be regarded with caution. Differences in experimental techniques and experimental errors may be responsible for the deviations between the data shown. The trends, however, appear to differ, and it is evident that further

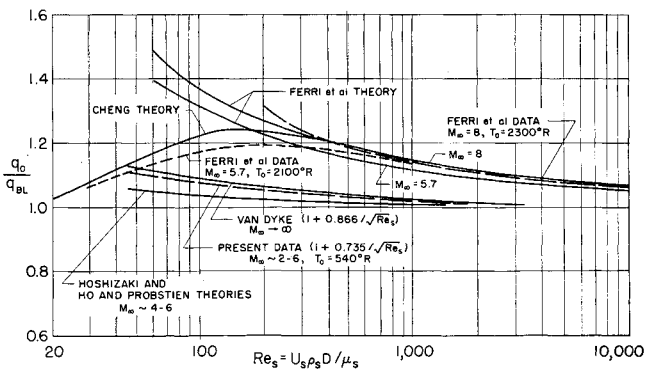

Fig. 14 Comparison of theoretical and experimental stagnation point heat transfer

investigations will be necessary to resolve the questions involved.

Turning to the local heat flux, Figs. 11–13 are summaries of the distributions over the spherical portion of the model. The glass model data and the nickel model data agree well up to $\theta \approx 80°$. The data scatter becomes progressively worse as θ approaches 90°, since the heat flux becomes quite small and experimental uncertainties become progressively more important. The local heat flux agrees well with Lees' theory for θ less than 45° and does not show any substantial Reynolds number dependence. The Mach 2 data agree with Lees' theory over the entire hemisphere; however, the Mach 4 and 6 data are somewhat higher than Lees' predictions for θ greater than 45°. This deviation corresponds to the pressure coefficient's deviation from the Newtonian distribution in these areas. It is surprising that the Mach 2 heat transfer data and pressure distribution data support a Newtonian distribution better than the Mach 4 and 6 data.

References

[1] Probstein, R. F., "Shock wave and flow field development in hypersonic re-entry," ARS J. **31,** 185–194 (1961).

[2] Hayes, W. D. and Probstein, R. F., *Hypersonic Flow Theory* (Academic Press, New York, 1959), p. 372.

[3] Hoshizaki, H., "Shock generated vorticity at low Reynolds numbers," Lockheed Missiles & Space Div. Rept. 48381, Vol. 1, pp. 9–43 (1959).

[4] Ho, H. T. and Probstein, R. F., *Rarefied Gas Dynamics* (Academic Press, New York, 1961), pp. 525–552.

[5] Cheng, H. K., "Hypersonic shock-layer theory of the stagnation region at low Reynolds number," *Proceedings of the 1961 Heat Transfer and Fluid Mechanics Institute* (Stanford University Press, Stanford, Calif., 1962), pp. 161–175.

[6] Ferri, A., Zakkay, V., and Ting, L., "Blunt body heat transfer at hypersonic speed and low Reynolds numbers," Polytech. Inst. Brooklyn, PIBAL Rept. 611 (1960); also J. Aerospace Sci. **28,** 962–971 (1961).

[7] Van Dyke, M., "Second-order compressible boundary-layer theory with application to blunt bodies in hypersonic flow," Stanford Univ., Aeronaut. Eng. Div. Rept. AFOSR-TN-61-1270 (1961).

[8] Ferri, A. and Zakkay, V., "Measurements of stagnation point heat transfer at low Reynolds numbers," Polytech. Inst. Brooklyn, ARL TR 38 (1961).

[9] Frössling, N., "Mass transfer, heat transfer and skin friction in two-dimensional and rotationally symmetrical laminar boundary layers," Natl. Advisory Committee for Aeronaut. Rept. TN-1462 (1958).

[10] Sibulkin, M. J., "Heat transfer near the forward stagnation point of a body of revolution," J. Aeronaut. Sci. **19,** 570–571 (1952).

[11] Fay, J. A. and Riddell, F. A., "Theory of stagnation point heat transfer in dissociated air," J. Aeronaut. Sci. **25,** 73–85 (1958).

[12] Lees, L., "Laminar heat transfer over blunt-nosed bodies at hypersonic flight speeds," Jet Propulsion **26,** 259–269, 274 (1956).

[13] Neice, S. E., Rutkowski, R. W., and Chan, K. K., "Stagnation-point heat-transfer measurements in hypersonic, low-density flow," J. Aerospace Sci. **27,** 387–388 (1960).

[14] Wilson, M. R. and Wittliff, C. E., "Low density stagnation point heat transfer measurements in the hypersonic shock tunnel," ARS J. **32,** 275–276 (1962).

[15] Maslach, G. J. and Sherman, F. S., "Design and testing of an axisymmetric hypersonic nozzle for a low density wind tunnel," Univ. Calif., Wright Air Dev. Div. TR 341 (1956).

[16] Owen, J. M. and Sherman, F. S., "Design, fabrication, and evaluation of a Mach 4 axially symmetric nozzle for rarefied gas flows," Univ. Calif., Eng. Project Rept. HE-150-104 (1952).

[17] Tewfik, O. K. and Giedt, W. H., "Heat transfer, recovery factor, and pressure distributions around a circular cylinder normal to a supersonic rarefied air stream," J. Aeronaut. Sci. **27,** 721–729 (1960).

[18] Hickman, R. S., "The influence of shock wave-boundary layer interaction on heat transfer to an axisymmetric body," Univ. Calif., Eng. Project Rept. HE-150-191 (1960).

[19] Hilsenrath, J., "Tables of thermal properties of gases," Natl. Bur. Standards Circular 564 (1956).

MARCH 1963 AIAA JOURNAL VOL. 1, NO. 3

An Integral Method for Calculation of Supersonic Laminar Boundary Layer with Heat Transfer on Yawed Cone

SHEE-MANG YEN* AND N. A. THYSON†

University of Illinois, Urbana, Ill.

An integral method for calculating the three-dimensional boundary layer over the surface of a cone at angle of attack is investigated. The numerical procedure of integration for that method on the basis of a simplifying assumption concerning the boundary layer development along the cone generator is developed and illustrated by applying the method to find the solutions of integral equations for a specific example. The results obtained for the example for the range of circumferential angle of 40° investigated are summarized and given as heat transfer coefficients, coefficients of friction, and other friction parameters. The distribution of heat transfer coefficients checked with available experimental data fairly well.

Nomenclature

a = shape parameter in longitudinal velocity profile
b = shape parameter in cross flow velocity profile
c = shape parameter in enthalpy profile
C = parameter in Chapman-Rubesin temperature-viscosity relation
c_f = coefficient of friction
c_p = specific heat at constant pressure
f_w'' = shear parameter
h = heat transfer coefficient
H = total enthalpy
K = proportionality parameter in transformed boundary layer thickness
St = Stanton number
T = temperature
T_1 = dimensionless external temperature ($1/T_1 = u_e^2/2c_pT_e$)
u = velocity in x direction (along a generator)
v = velocity in y direction (perpendicular to surface of a cone)
w = velocity in circumferential direction
x = coordinate along generator

Received by IAS August 27, 1962; revision received January 7, 963.

* Associate Professor of Aeronautical and Astronautical Engineering.

† Formerly Graduate Student; now with Avco Corporation.